

Article

Suitability of Different Blood-Analogous Fluids in Determining the Pump Characteristics of a Ventricular Assist Device

Finn Knüppel , Inga Thomas, Frank-Hendrik Wurm and Benjamin Torner * 

Institute of Turbomachinery, University of Rostock, Albert-Einstein-Straße 2, 18059 Rostock, Germany; finn.knueppel@uni-rostock.de (F.K.)

* Correspondence: benjamin.torner2@uni-rostock.de

Abstract: Ventricular assist devices (VADs) are implantable turbomachines that save and improve the lives of patients with severe heart failure. In the preclinical evaluation, a VAD design must be experimentally or numerically tested regarding its pump characteristics, primarily for its pressure buildup (pressure head H) since it must provide the cardiovascular system with a sufficient blood flow rate Q . Those pump characteristics are determined on a test bench. Here, a glycerol-water mixture is almost exclusively used as blood-analogous fluid, which should reflect the properties (density, viscosity) of blood as close as possible. However, glycerol water has some disadvantages, such as a higher density compared to real blood and a relatively high cost. Therefore, the study aimed to analyze six different blood analogous fluids to select the most suitable one in consideration of fluid handling, costs, and, most importantly, fluid properties (material and rheological). First, all fluids were mixed to achieve reference values of blood density and viscosity from the literature. Afterwards, the pump characteristics (pressure heads and efficiencies via the VAD) were experimentally and numerically determined and compared among each other and with literature values. Of all six investigated fluids, only the aqueous–polyethylene glycol 200 (PEG 200) solution matches exactly the desired blood properties, and the pump characteristics of this fluid are in the expected range for the analyzed operation point of the VAD. Another advantage is that the cost of the mixture is 35% lower compared to glycerol water. Additionally, we demonstrate that non-Newtonian flow behavior has little effect on the pump characteristics in our VAD.



Citation: Knüppel, F.; Thomas, I.; Wurm, F.-H.; Torner, B. Suitability of Different Blood-Analogous Fluids in Determining the Pump Characteristics of a Ventricular Assist Device. *Fluids* **2023**, *8*, 151. <https://doi.org/10.3390/fluids8050151>

Academic Editors: Eldad Avital and D. Andrew S. Rees

Received: 17 March 2023

Revised: 28 April 2023

Accepted: 1 May 2023

Published: 11 May 2023



Copyright: © 2023 by the authors. Licensee MDPI, Basel, Switzerland. This article is an open access article distributed under the terms and conditions of the Creative Commons Attribution (CC BY) license (<https://creativecommons.org/licenses/by/4.0/>).

Keywords: blood-analogous fluid; blood pump; ventricular assist device; pump characteristics; pressure head; efficiency; density; viscosity; glycerol; polyethylene glycol

1. Introduction

Heart failure is a cardiovascular disease with an increasing worldwide prevalence every year [1]. If the disease is too severe, a heart transplantation is the gold standard for treatment. However, a pronounced donor heart shortage exists. For example, Germany recorded 329 transplants compared to 727 patients on the waiting list at the end of 2021 [2]. This urges the development of technical solutions, such as implantable ventricular assist devices (VADs). These devices maintain the blood circulation in the diseased body; in other words, they lead to an increase in blood pressure Δp to compensate for vessel resistance and achieve a desired flow rate Q in the cardiovascular system.

The majority of implanted VADs operate according to the turbopump principle [3], and the operating range results from the requirement to maintain the blood flow. For this purpose, a defined head H must be built up at a certain blood flow rate Q under the condition of the highest possible efficiency η_i . The head H is calculated by the pressure increase Δp via the VAD (Equation (1)) and is given in [mmHg] as a standard practice in medicine. (Please note that 7.5 mmHg equals 1 kPa, and that the head is defined differently for standard industrial turbopump application [4].)

$$H = \frac{\Delta p}{133.3} \text{ [mmHg]} \quad (1)$$

The inner efficiency η_i of the VAD in Equation (2) is the ratio between the useful fluid power ($\Delta p \cdot Q$) and the internal power ($M \cdot 2\pi n$) at the impeller blades and is stated generally in [%].

$$\eta_i = \frac{\Delta p \cdot Q}{M \cdot 2\pi n} \cdot 100 \text{ [%]} \quad (2)$$

Whether a VAD meets these requirements can be checked by determining the head characteristic $H = f(Q)$ and efficiency characteristics $\eta_i = f(Q)$. These two variables represent the so-called pump characteristics [4]. Pump characteristic investigations are performed either in vitro (on the test bench) or in silico (using flow simulations) in the preclinical evaluation of a VAD [5–8]. Here, a blood-analogous fluid (BAF) is used for in-vitro and in-silico studies of the VAD's pump characteristics. These BAFs shall mimic the fluid properties (density ρ , dynamic viscosity μ) of the blood as close as possible. Furthermore, a third, important fluid property can be derived from these variables—the kinematic viscosity $\nu = \mu/\rho$.

There are two reasons why it is important to mimic the fluid properties of blood as close as possible with a BAF when analyzing the flow in a VAD.

The first reason is that deviations in kinematic viscosity between BAF and blood will also alter the Reynolds number in the VAD flow since Re depends on the kinematic viscosity ν . This relation can be observed in the pump's Reynolds number Re_p (Equation (3)), which is a characteristic Reynolds number of a turbomachine. Re_p consists of the circumferential velocity u_c and the diameter D_c at the impeller's casing and the kinematic viscosity ν .

$$Re_p = \frac{u_c \cdot D_c}{\nu} \quad (3)$$

Here, the Reynolds number should be identical between a VAD operating with a blood-analogous fluid (in vitro on the test bench) and a VAD operating with blood (in vivo in the patient) since preliminary investigations in industrial turbopumps have shown that the efficiency η_i can deviate markedly in a turbopump operating with different kinematic viscosities in Figure 13.9 in Ref. [4].

The second reason for the same fluid properties is that differences in densities ρ between BAF and blood will also lead to a difference in pressure heads H . This can be explained by expanding Equation (1) with Euler's turbomachinery equation. In doing so, Equation (4) arises where the pressure increase Δp can be expressed by the angular momentum balance, which is connected with the velocities in the VAD. The velocities in Equation (4) are the circumferential velocity u (which is uniform on a specific radius for an axial VAD) and the increase of the circumferential component of the velocity in the absolute frame Δc_u between impeller inlet and impeller outlet.

$$H = \frac{\Delta p}{133.3} \text{ [mmHg]} = \frac{\rho (u \cdot \Delta c_u)}{133.3} \text{ [mmHg]}. \quad (4)$$

If velocities u and c_u are the same between BAF and blood in the VAD (which could be a valid assumption, as will be shown later), a difference in density ρ will lead to a deviation in head H .

For these two reasons, it is obvious that the consistency of the fluid properties is an important factor for the correct determination of the pump characteristics of the VAD in in-vitro and in-silico studies so that similar pump characteristics exist in the VAD on the test bench and in the implanted VAD.

Regarding this, the most used BAF for determining the pump characteristics in VADs is a Newtonian glycerol–water mixture [5–12]. Advantages of this mixture over other BAFs, such as polyacrylamide [13,14] or diethylphthalate–ethanol [15] mixtures, are the low toxicity, easy handling, and good replication of the blood viscosity. Nevertheless, the density ρ of glycerol water is higher than those of blood when both fluids have the same dynamic viscosity μ . This leads to changes in density, kinematic viscosity, and Re_p between the glycerol water and blood, as can be seen in Table 1. According to the above, differences

in pumping characteristics between a VAD operating with glycerol water and blood are to be expected.

Table 1. Comparison in fluid properties and Reynolds numbers between BAF (glycerol water) and blood (typical values from literature studies [16–18] were taken). The pump’s Reynolds number was calculated for the VAD under investigation, displayed in Figure 1.

Fluid	Density [kg/m ³]	Dynamic Viscosity [mPas]	Kinematic Viscosity [mm ² /s]	Re _p [–]
Blood (typical values from literature studies)	1050	3.5	3.33	31,770
Glycerol water (37.5/63.5%, v/v)	1100 (+5%)	3.5 (±0.0%)	3.18 (–5%)	33,000 (+5%)

The questions, therefore, arise as to how these different fluid properties affect the pump characteristics and—if differences in pump characteristic are noticeable—whether there is an alternative BAF that better replicates the fluid properties of blood than glycerol water but is at least equivalent in manageability, storage, and cost. Regarding this, some promising investigations with mixtures based on propylene–glycol water and polyethylene–glycol water were made [19–21]. Unfortunately, none of these mixtures have been used as BAFs for in-vitro determination of the pump characteristics in VADs so far.

Hence, the aim of this study was to test different Newtonian BAFs regarding their ability to match fluid properties of blood, as well as their suitability in determining the pump characteristics for in-vitro and in-silico studies. First, four Newtonian BAFs were selected and mixed to reach reference fluid properties of porcine blood from literature studies. Afterwards, these BAFs were used to determine the pressure head of a VAD on a test bench. Furthermore, the fluid properties were included in CFD simulations of the same VAD to account for the pressure heads, as well as the VAD’s efficiency. The selection of the most appropriate BAF was made based on these results, as well as a consideration regarding fluid handling and costs.

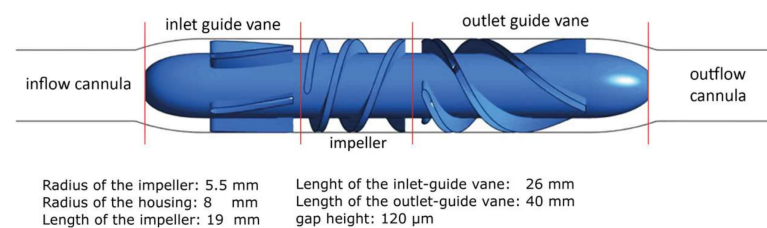


Figure 1. VAD geometry with important geometric information. The figure is taken from Ref. [18].

2. Methods

2.1. Material and Rheological Properties of the Fluids

In total, four Newtonian BAFs were examined. The fluids intend to reflect the fluid properties of the blood in a VAD flow as close as possible. By this, it is meant that a proper blood-analogous fluid should mimic the density as well as the viscosity of blood under high shear conditions, as they are present in VADs. The nearly constant dynamic viscosity μ of blood at high shear rates is considered as the first, important fluid property. The second fluid property is the fluid density ρ . These fluid properties were set to $\mu \approx 4.0$ mPas and $\rho \approx 1062$ kg/m³ as the desired reference values in this study. These values were taken from the studies of Refs. [22,23], which investigated the fluid properties of porcine blood. Porcine blood is like human blood in its properties [24] and is often used for in-vitro measurements with blood in VADs [25–28].

The BAFs are summarized in Table 2. First, a glycerol–water mixture was taken, which has been used almost exclusively as BAF in experimental VAD research so far [5–12,29].

Additionally, three further aqueous mixtures based on polyethylene glycol (PEG) and ethylene glycol have been investigated. These three fluids are Newtonian fluids and have not been used for in-vitro studies of VADs so far.

Table 2. Investigated Newtonian blood-analogous fluids.

Fluid	Rheological Evaluation	Experimental Evaluation	Numerical Evaluation
Glycerol water (G-W)	✓	✓	✓
PEG 200-water (PEG200-W)	✓	✓	✓
Ethylene glycol-water (EG-W)	✓	✓	✓
PEG 8000-water (PEG8000-W)	✓	✓	✓

The kinematic viscosity ν of the Newtonian fluids was measured using an Ubbelohde viscometer (number 32,026; Paragon Scientific, Prenton, UK). The measurement accuracy is $\pm 0.17\%$. Hydrometers (Carl Roth GmbH, Karlsruhe, Germany) with a measuring range of $\rho = (1000 - 1200) \text{ kg/m}^3$ were used to determine the density. The temperature was set to $(25 \pm 0.1) \text{ }^\circ\text{C}$. At each measuring point, 10 values were taken and averaged for 30 s. Every measurement was repeated five times to minimize random errors.

2.2. Experimental VAD Setup for Determining the Pump Characteristics

The pressure head H was experimentally determined for a VAD using different BAFs. Therefore, the VAD was integrated in a test bench, as shown in Figure 2. The test bench was constructed according to the guidelines of DIN EN ISO 9906 [30]. The VAD is an axial turbopump, designed by our institute for research (shown in Figure 2). A full-size model was made of acrylic material as a research device. The design rationale is explained in Ref. [16]. The VADs operate at a chosen nominal operation point ($Q = 4.5 \text{ L/min}$, $n = 7900 \text{ 1/min}$) to achieve a desired design pressure head of $H \approx 74 \text{ mmHg}$.

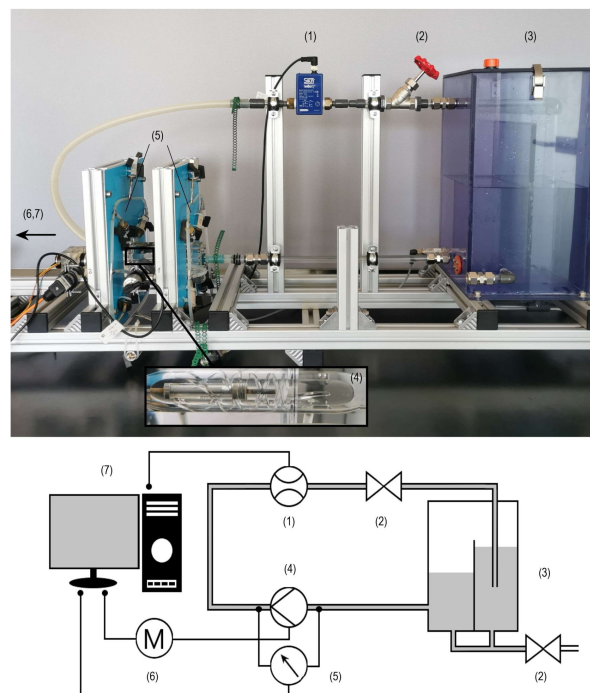


Figure 2. Test bench with flow-rate sensor (1), throttle (2), volume reservoir (3), VAD (4), pressure sensors (5), motor with coupling (6), and computer with measuring and control system (7).

An electric motor (3564K024B; Faulhaber, Schönaich, Germany) drives the impeller. A digital flow-rate sensor (VMI07, SIKA GmbH, Kaufungen, Germany) monitors the flow rate in the test bench, which can be adjusted by a throttle. Two relative pressure sensors (sensor 1: DMU 0,25 ES; Landefeld, Kassel, Germany; sensor 2: P-31-R; WIKA, Klingenberg, Germany) at four positions along the perimeter before and behind the VAD were used to measure the VAD's pressure head H . Eight measurements per fluid (one minute per measurement) were carried out, whilst control measurements of density and viscosity were taken between the measurements.

2.3. Numerical VAD Setup for Determining the Pump Characteristics

Besides the experimental analysis of the pressure heads, the blood-analogous fluids were also investigated numerically. Therefore, the pressure head H , as well as the inner efficiency η_i , was determined for the different BAFs. For these in-silico investigations, large eddy simulations (LES) were performed using ANSYS CFX 2022R2 (Ansys Inc., Canonsburg, PE, USA). The LES method was chosen to compute a certain amount of the turbulent flow field directly. Previous work of the authors indicates that this is needed to guarantee that the flow of the VAD is computed in a proper way [16,18]. The computational domain includes all hydraulic parts of the VAD (a part of the domain is shown in Figure 1) and has a size of approximately 19.4 million cells. Grid quality criteria regarding angles, volume changes, and aspect ratios were kept in recommended ranges [31]. Furthermore, y_1^+ -values were kept at around one (time- and space-averaged values at the blades) and three (maximal value in the domain). Boundary conditions were set as follows: A zero pressure was set as the inlet condition, and a constant flow rate of $Q = 4.5$ L/min was defined at the outlet. The rotor speed was equivalent to the experiments with $n = 7900$ 1/min. During the simulations, root-mean-square residuals dropped below 10^{-5} . Verification of the grid and the numerical setup is provided in Supplementary Materials, where it is shown that the head, as well as the analyzed turbulent flow variable, can be reproduced adequately on this mesh size.

The impeller rotated with a time step equal to a rotor increment of 1° , and the total simulation time corresponds to 10 rotor revolutions. Time averaging for the pressure heads and efficiencies were done for the last five impeller revolutions.

The densities and dynamic viscosities, which were determined from the investigations in Section 3.1, were specified as fluid properties to describe the behavior of the different BAFs.

Furthermore, a reference simulation (named as "Reference A") was performed, which "mimicked" the fluid properties of blood flow from the literature. This is a simulation of the VAD with the constant viscosity $\mu = 4$ mPas and a density of $\rho = 1062$ kg/m³ for porcine blood from Ref. [23].

3. Results and Discussion

3.1. Fluid Properties for the Newtonian Blood-Analogous Fluids

The viscosities of the Newtonian BAFs are shown in Table 3. The standard deviation of all measurement series is <0.05 . All BAFs achieve the desired dynamic viscosity of $\mu = 4$ mPas, but some mixtures have larger deviations to the blood density of $\rho = 1062$ kg/m³. Just the PEG 200-water mixture reached this desired density. The highest deviations in density were found in glycerol water with $\rho = 1110$ kg/m³ and PEG 8000-water with $\rho = 1012$ kg/m³. Both have a relative deviation of $\approx 5\%$ to the fluid properties of blood from Reference A.

Table 3. Measured densities and viscosities for a specific mixing ratio and a temperature of 25 °C. The relative deviation to Reference A ($H_{ct} \approx 40\%$) is given.

Fluid	Volume Ratio [v/v,%]	Density ρ [kg/m ³]	Dynamic Viscosity [mPas]	Kinematic Viscosity [mm ² /s]
Blood—Reference A [23]	-	1062	4.00	3.77
G-W	40.7/59.3	1110 (+4.5%)	4.00 ($\pm 0.0\%$)	3.60 (−4.5%)
PEG200-W	38.0/62.0	1060 (−0.2%)	3.99 (−0.3%)	3.76 (−0.1%)
EG-W	56.0/44.0	1072 (+0.9%)	3.96 (−1.0%)	3.69 (−2.1%)
PEG8000-W	08.0/92.0	1012 (−4.7%)	3.93 (−1.7%)	3.88 (+2.9%)

3.2. Experimental and Numerical Results for the Newtonian Blood-Analogous Fluids

The experimentally and numerically determined heads H and efficiencies η_i are summarized in Table 4. The heads from experiments and simulations were combined in one column since they show similar results for each fluid (relative deviation $\leq 5\%$ between EXP and CFD).

Table 4. Heads H and efficiencies η_i of the VAD from the experiments and the flow simulations. The results are compared to the pump characteristics of a reference simulation, which uses the fluid properties of blood from Reference A. In addition, the costs for one liter of mixed fluid are stated. The measurement uncertainty for all measured data in the test rig is maximal $\pm 3.0\%$.

Fluid	Head H (CFD EXP) [mmHg]		Efficiency η_i (CFD) [%]	Costs per Liter [€/L]	Density ρ [kg/m ³]	Kin. Viscosity [mm ² /s]
Blood—Reference A [23]	73.8	-	31.8	-	1062	3.77
G-W	77.3	74.6	32.0	22.90	1110	3.60
EG-W	74.5	71.1	31.7	14.55	1072	3.69
PEG200-W	73.6	74.9	31.6	14.81	1060	3.76
PEG8000-W	69.8	67.9	31.1	04.52	1012	3.88

PEG8000-W achieved the lowest pressure head with $H = (67.9 - 69.8)$ mmHg, which is a deviation of around -8% to the reference pressure head of $H = 73.8$ mmHg. The results of the EG-W and PEG200-W are similar and vary around the desire head of ≈ 74 mmHg. A slight overprediction up to $+5\%$ compared to Reference A is found with the glycerin–water mixture.

Here, it is noticeable that the heads are primarily influenced by the density, with pressure heads from the simulation increasing with denser fluid. (Please note: this linear trend is not as clearly visible in the experiments as in the CFD due to measurement uncertainties). This dependency has been explained already by theoretical considerations by Equation (4) and is demonstrated again with the results for the fluids with the lowest density (PEG800-W) and the highest density (G-W) in Table 5.

Table 5. Deviations of density and head between glycerol water (G-W, highest density) and PEG 8000-water (PEG8000-W, lowest density). An averaged value for the head from Table 4 is used.

Fluid	Head H [mmHg]	Density ρ [kg/m ³]
G-W	76.0	1110
PEG8000-W	68.9	1012
Rel. Dev. [%]	$\approx 10\%$	$\approx 10\%$

The differences in head can also be seen in the local pressure field, which is displayed in the upper subplot in Figure 3. This subplot shows a cylindrical cut in the pressure field

through the inlet guide vane, the impeller, and the outlet guide vane at a radius r of 80 % in relation to the casing's radius R_c .

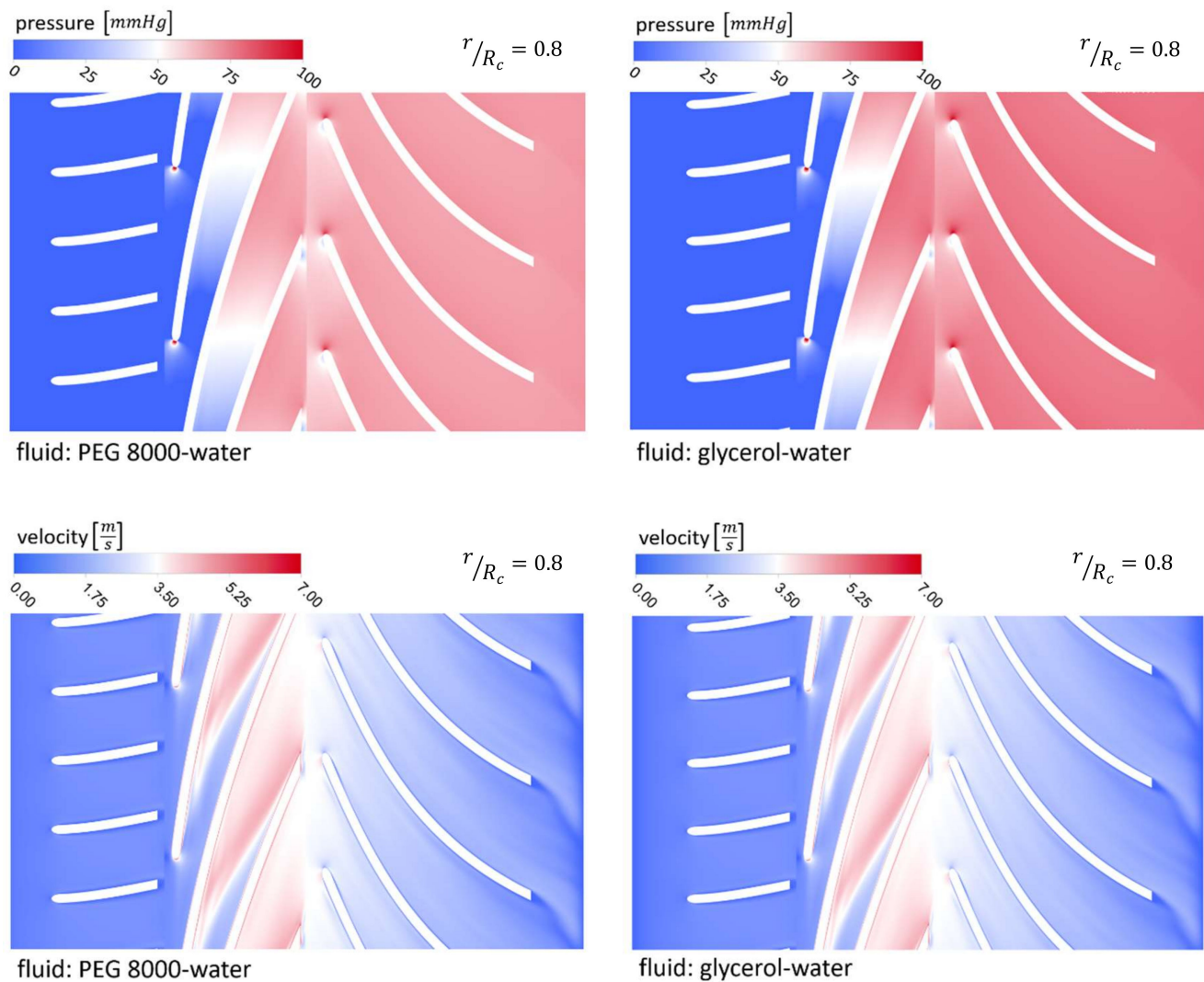


Figure 3. Time-averaged visualization of the pressures and velocities of simulations with the fluid properties of PEG 8000-W (left side) and G-W (right side). Visualized in a cylindrical cut through the impeller and outlet guide vane at a radius r of 80% ($r = 0$ is at the hub) in relation to the casing radius r_c .

Since the pressures varied markedly between G-W (highest density) and PEG8000-W (lowest density), potential differences in fluid velocity were investigated as well. The velocity fields are displayed in the bottom subplots in Figure 3. Here, no marked differences in velocities exist between G-W and PEG8000-W. This is also the case for all simulations with all the other BAFs (not displayed here). The reason for the uniform velocities can be explained by the Euler (momentum) Equation (5) for an incompressible fluid in a steady state condition:

$$c_j \frac{\partial c_i}{\partial x_j} = \frac{1}{\rho} \frac{\partial p}{\partial x_i}. \tag{5}$$

The left term in Equation (5) describes the inertia of the flow (dependent on the velocities c_i, c_j), which is balanced by the density-normalized pressure gradients on the right-hand side. Considering that an increase in density cancels an increase in the pressure gradient on the right-hand side, similar inertia terms and, hence, velocity fields between two fluids with different densities can be explained.

Furthermore, the efficiencies are compared between all BAFs in Table 4. As with the velocities, the efficiencies in the VAD are similar with $\eta_i \approx (31 - 32)\%$ for all BAFs. Here, no noticeable influence of the kinematic viscosity on the efficiency is evident. The kinematic viscosities in our analysis differ to less—with a maximum of 8% between PEG8000-W and G-W—to change the flow field and, hence, the pump's efficiency markedly.

When comparing the BAFs among each other, the economical factor is also relevant since a large amount of fluid ($V > 10$ liter in our case) is used in the measurement campaigns. The cost for one liter of each solution is given in Table 4. PEG8000-W is the cheapest and G-W the most expensive fluid. The costs for EG-W and PEG 200-W are relatively similar and fluctuate within a range of EUR 14 to 15/L.

4. Comparison of the Pump Characteristics between Newtonian & Non-Newtonian Fluids

Up to this point, we have assumed that the fluid properties of blood are invariant from the shear rate of the VAD's flow, which means a Newtonian flow behavior. The reason for this assumption is that preliminary studies have shown that blood has a nearly constant viscosity μ at high shear rates above $S_{ij} \approx 100$ 1/s [32]. These shear rates are exceeded in most parts of the VAD [16], which is the reason for the Newtonian fluid assumption in most in-vitro and in-silico investigations, e.g., in [17,33]).

Nevertheless, blood generally has a strong non-Newtonian character due to its shear-thinning behavior, and there are several areas in the VAD where this Newtonian assumption strictly does not hold. This can be seen from Figure 4, where volumes with shear rates $S_{ij} < 150$ 1/s are present in the inlet cannula and inlet guide vane of the axial VAD under investigation. A non-Newtonian flow behavior might be present in this inlet region, and the entire VAD flow (and, hence, the pump characteristics) could be affected by this non-Newtonian behavior since all flow from the inlet region enters the subsequent rotating impeller.

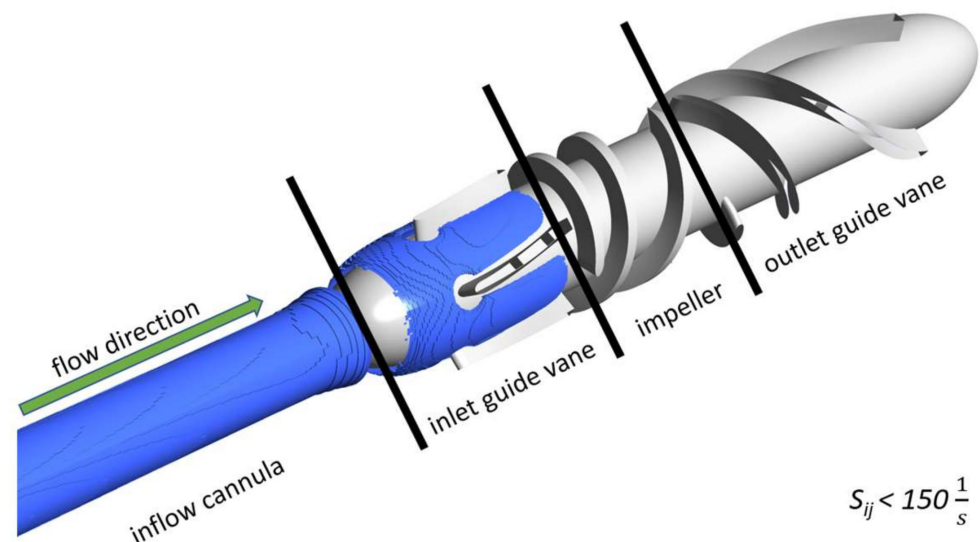


Figure 4. Areas in the VAD where the shear rates are below the threshold of $S_{ij} < 150$ s⁻¹. The flow was computed by a large eddy simulation (from Ref. [18]) with fluid properties of a glycerol–water mixture.

Hence, it seems interesting to analyze if non-Newtonian fluid effects have an influence on the pump characteristics in the VAD. Therefore, two non-Newtonian BAFs were also mixed (see Table 6), and their pump characteristics were compared experimentally and numerically with the pump characteristics of their Newtonian equivalents.

Table 6. Measured densities and dynamic viscosities of the non-Newtonian BAFs (at a measuring shear rate of 2000 s^{-1}) for a specific mixing ratio and a temperature of $\theta = 25^\circ \text{C}$. The viscosities were compared at high shear rates to the dynamic viscosity of Ref. [22] ($H_{ct} \approx 40\%$). The density was compared to the density value of Ref. [23] ($H_{ct} \approx 40\%$).

Fluid	Ratio of the Newtonian Components [$v/v, \%$]	Xanthan Gum [$w/w, \%$]	Density ρ [kg/m^3]	Dynamic Viscosity [mPas]
Blood—Reference A [23]	-	-	1062	-
Blood—Ref. [22]	-	-	-	3.80
G-W-X (non-Newtonian)	35.0/65.0	0.01	1093	3.70
PEG200-W-X (non-Newtonian)	33.0/67.0	0.01	1053	3.78

4.1. Methods for the Non-Newtonian Fluid Analyses

To create these non-Newtonian fluids, Xanthan gum was added to the glycerol-water (G-W) and PEG 200-water (PEG200-W) solution by precise scaling (CX-128; Homgeek; accuracy: $\pm 0.001 \text{ g}$). A HAAKE Mars II rheometer (Thermo Scientific, Waltham, MA, USA) was utilized to measure the viscosity of the non-Newtonian fluids over a broad range of shear rates between $S_{ij} = (1 - 2000) \text{ s}^{-1}$. A double-cone geometry (DC60/1° Ti L L09 008) with the corresponding measuring plate attachment (MP-DC 60b) was used, which is especially suitable for measuring low viscosity fluids [34].

The CFD setup is identical to the previously described one. Just for the fluid properties, functions of the dynamic viscosity depending on the shear rate $\mu = f(S_{ij})$ were created based on the experimental fluid measurements from Table 6 and Figure 5.

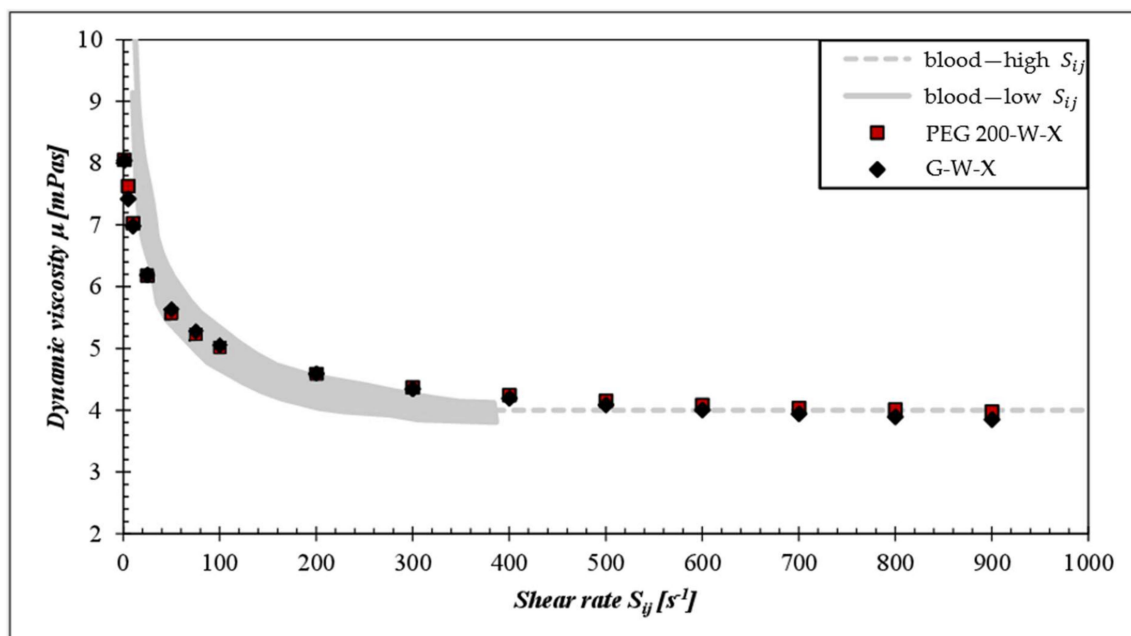


Figure 5. Shear-rate dependent dynamic viscosities $\mu = f(S_{ij})$ for the mixtures of G-W-X and PEG200-W-X compared to the reference range of porcine blood [22,23].

4.2. Results for the Non-Newtonian Fluid Analyses

Figure 5 illustrates the measured viscosity curves of the non-Newtonian blood analogous fluids. These are compared to Ref. [22], which measured the shear-dependent viscosity curve for porcine blood at $H_{ct} \approx 40\%$. Both fluids are within the grey area, which reflects

the lower and upper bounds of the shear-dependent viscosity from Ref. [22] and fits the asymptotic reference value in that figure. The densities of the non-Newtonian fluids are also shown in that table, with PEG200-water matching the reference density of blood from Ref. [23].

The numerically and experimentally determined pump characteristics of the non-Newtonian fluids are compared to their Newtonian equivalents in Table 7. There are no noticeable differences in the pressure heads or efficiencies between the Newtonian and non-Newtonian fluids. Both exhibit the same trends experimentally as well as numerically. This is also evident in the LES pressure and velocity plots in Figure 6.

Table 7. Pressure heads and efficiencies of the VAD determined by experiments and flow simulations.

Fluid	Pressure Head [mmHg]		Efficiency (CFD) [%]
	EXP	CFD	
G-W (Newtonian)	74.6	77.3	32.0
G-W-X (non-Newtonian)	74.0	76.9	32.8
PEG 200-W (Newtonian)	74.9	73.6	31.6
PEG200-W-X (non-Newtonian)	73.6	73.0	32.0

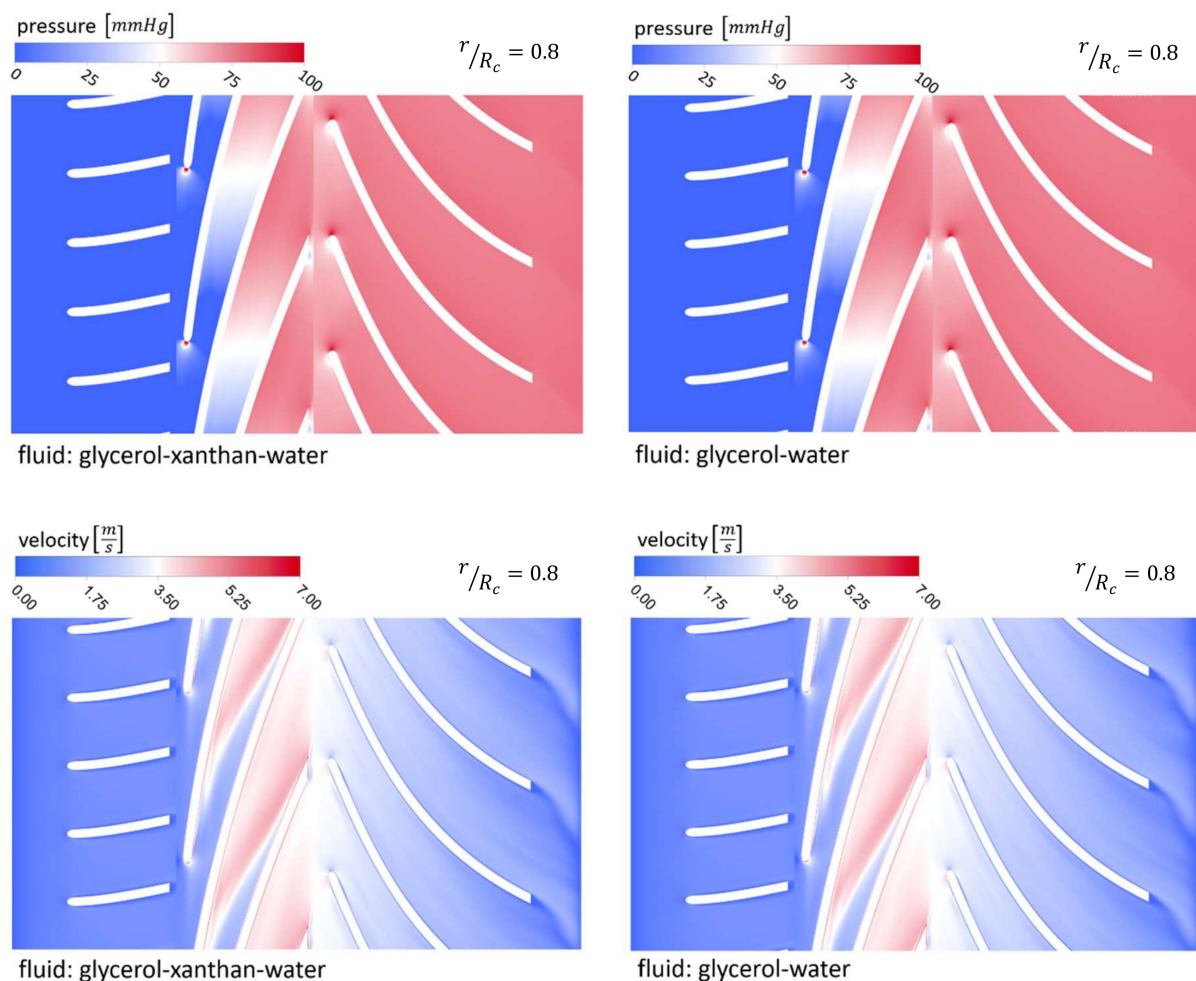


Figure 6. LES-plots of the pressure and the velocity fields of glycerol–xanthan water (left side) and glycerol water (right side).

5. Selection to Find the Most Suitable Blood-Analogous Fluid

At first, it can be stated that there is little difference in the pump characteristics between the Newtonian and non-Newtonian fluids, as can be seen from Table 7. This is consistent with the assumption that blood has a nearly constant viscosity in high-shear regions [32], and a Newtonian flow behavior can be assumed for in-vitro or in-silico studies of the pump characteristics in VADs [5–8,17,33].

Except for PEG8000-W, all experimentally and numerically analyzed BAFs manage to achieve a desired pressure head of $H \approx 74$ mmHg with a relative deviation of maximum 5% to this reference value (see Table 4). Furthermore, the velocities and efficiencies are similar between all investigated BAFs. Therefore, we can conclude that all fluids based on glycerol, PEG-200, and ethylene glycol mixtures seem appropriate for in-vitro or in-silico examinations of the VAD's pump characteristics. Hence, other factors will lead to the selection of the most suitable fluid.

For the final selection, costs seem to also be an important influential factor. The most used fluid to date, glycerol water has the highest costs, whereas the fluids with PEG200 and EG are less expensive (see Table 4). In addition, the fluid properties of blood, such as density and dynamic viscosity, can also be reproduced much better with the PEG200 and EG mixtures. PEG-200 water achieves exactly the defined values: a viscosity of $\mu = 4$ mPas and a density of $\rho = 1060$ kg/m³. The second closest is EG-W with a density of $\rho = 1072$ kg/m³. However, we do not recommend the use of the ethylene glycol solutions due to the much higher toxicity compared to PEG200 or glycerol mixtures [35]. Therefore, we found PEG200-water as the best choice for a BAF when the pump characteristics are investigated in VADs.

6. Conclusions

The purpose of this study was to find a blood-analogous fluid that imitates the fluid properties of blood flows at high shear rates, such as they exist in ventricular assist devices. Four Newtonian and two non-Newtonian fluids were prepared and investigated. After their dynamic viscosities matched the desired blood viscosity of $\mu = 4$ mPas, the pressure heads H of a VAD with the respective fluid was experimentally assessed on a test bench. Furthermore, numerical studies were conducted to account for more pump characteristics, such as the efficiency η_i of the VAD.

The desired dynamic viscosity could be achieved by all fluids. Nevertheless, this caused noticeable differences in densities. Only the polyethylene glycol 200 mixture matches the desired density ($\rho = 1060$ kg/m³) and viscosity at a volumetric mixing ratio of 62:38%. The commonly used glycerol–water solution, the current standard for in-vitro testing of VAD performances, was furthest from the desired density value with $\rho = 1110$ kg/m³. The pressure heads, efficiencies, and velocity fields were comparable between the glycerol–water and PEG 200–water mixture. In addition, the good manageability and low toxicity of PEG200-W is comparable to that of glycerol. Nevertheless, the costs of glycerol-water are more than 35% higher compared to PEG200-W. Considering all of the stated reasons, PEG-200-water seems to be the most suitable blood-analogous fluid to investigate pump characteristics in VADs.

Supplementary Materials: The following supporting information can be downloaded at: <https://www.mdpi.com/article/10.3390/fluids8050151/s1>, Figure S1: Analysis of flow variables on different grid sizes. Left: Pressure head H . Right: Volume-integrated, resolved turbulent kinetic energy k in the impeller domain. The red dot indicates the solution on the grid which was applied for the analysis.

Author Contributions: Conceptualization, F.K., I.T. and B.T.; Methodology, F.K. and I.T.; Software, I.T. and B.T.; Validation, B.T.; Formal Analysis, F.K., I.T. and B.T.; Investigation, F.K., I.T. and B.T.; Writing—Original Draft Preparation, F.K. and I.T.; Writing—Review & Editing, F.-H.W. and B.T.; Visualization, I.T.; Supervision, F.-H.W. and B.T.; Project Administration, F.-H.W. All authors have read and agreed to the published version of the manuscript.

Funding: Funded by the German Research Foundation (DFG)—Project number: 469384587.

Data Availability Statement: The data presented are freely available in this article and in the attached supplementary material. If more data is of interest, please feel free to request it from the corresponding author.

Conflicts of Interest: The authors declare no conflict of interest.

Nomenclature

c	velocity, m/s
D	diameter, m
H_{ct}	hematocrit, %
H	pressure head, mmHg
k	turbulent kinetic energy, m^2/s^2
M	impeller torque, Nm
n	rotational speed, 1/s
p	pressure, Pa
Q	flow rate, m^3/s
r, R	radius, m
Re_p	pump Reynolds number, –
S_{ij}	rate-of-strain tensor, 1/s
SUB-, SUPERSCRIPTS AND OPERATORS	
c	at the casing (for axial VADs)
x, j	spatial directions
v/v	volumetric share
w/w	mass share
Δ	increase
$\langle \dots \rangle$	time-averaged
l	fluctuation
u	circumferential velocity, m /s
V	volume, m^3
x	direction, m
η_i	inner efficiency, %
θ	temperature, $^{\circ}C$
μ	dynamic viscosity, Pa·s
ν	kinematic viscosity, m^2/s
ρ	density, kg/m^3
ABBREVIATIONS	
BAF	blood-analogous fluid
CFD	computational fluid dynamics
EXP	experiment
G	glycerol
LES	large-eddy simulation
PEG 200	polyethylene glycol 200
PEG 8000	polyethylene glycol 8000
Rel. Dev.	relative deviation
X	xanthan
W	water

References

- Gomar, F. Global epidemiology and future trends of heart failure. *AME Med. J.* **2020**, *5*, 1–6.
- Waage, P.; Kreuter, D.P.; Blome, B. Annual Report—Organ Donation and-Transplantation in Germany; Deutsche Stiftung Organtransplantation. 2021. Available online: <https://dso.de/SiteCollectionDocuments/DSO-Jahresbericht%202021.pdf> (accessed on 17 January 2023).
- Teuteberg, J.J.; Cleveland, J.C.; Cowger, J.; Higgins, R.S.; Goldstein, D.J.; Keebler, M.; Kirklin, J.K.; Myers, S.L.; Salerno, C.T.; Stehlik, J.; et al. The Society of Thoracic Surgeons Intermacs 2019 annual report: The changing landscape of devices and indications. *Ann. Thorac. Surg.* **2020**, *109*, 649–660. [[CrossRef](#)] [[PubMed](#)]
- Gulich, J.F. *Centrifugal Pumps*; Springer: Berlin/Heidelberg, Germany, 2014.
- Wu, Z.J.; Gottlieb, R.K.; Burgreen, G.W.; Holmes, J.A.; Borzelleca, D.C.; Kameneva, M.V. Investigation of fluid dynamics within a miniature mixed flow blood pump. *Exp. Fluids* **2001**, *31*, 615–629. [[CrossRef](#)]

6. Mizunuma, H.; Nakajima, R. Experimental study on shear stress distributions in a centrifugal blood pump. *Artif. Organs* **2007**, *31*, 550–559. [[CrossRef](#)] [[PubMed](#)]
7. Throckmorton, A.L.; Untaroiu, A.; Allaire, P.E.; Wood, H.G.; Lim, D.S.; McCulloch, M.; Olsen, D.B. Numerical design and experimental hydraulic testing of an axial flow ventricular assist device for infants and children. *ASAIO J.* **2007**, *53*, 754–761. [[CrossRef](#)]
8. Thamsen, B.; Mevert, R.; Lommel, M.; Preikschat, P.; Gaebler, J.; Krabatsch, T.; Kertzsch, U.; Hennig, E.; Affeld, K. A two-stage rotary blood pump design with potentially lower blood trauma: A computational study. *Int. J. Artif. Organs* **2016**, *39*, 178–183. [[CrossRef](#)]
9. Boes, S.; Thamsen, B.; Haas, M.; Daners, M.S.; Meboldt, M.; Granegger, M. Hydraulic Characterization of Implantable Rotary Blood Pumps. *IEEE Trans. Biomed. Eng.* **2018**, *66*, 1618–1627. [[CrossRef](#)]
10. Strauch, C.; Escher, A.; Wulff, S.; Kertzsch, U.; Zimpfer, D.; Thamsen, P.U.; Granegger, M. Validation of Numerically Predicted Shear Stress-dependent Dissipative Losses Within a Rotary Blood Pump. *ASAIO J.* **2021**, *67*, 1148–1158.
11. Su, B.; Chua, L.P.; Wang, X. Validation of an axial flow blood pump: Computational fluid dynamics results using particle image velocimetry. *Artificial Organs*. **2012**, *36*, 359–367. [[CrossRef](#)]
12. Mapley, M.C.; Seah, E.P.; Semenzin, C.; Wu, E.; Pauls, J.P. Analysis of the HeartWare HVAD pump characteristics under pulsatile operation. *Biomed. Signal Process. Control* **2021**, *68*, 102754. [[CrossRef](#)]
13. Mann, D.E.; Tarbell, J.M. Flow of non-newtonian blood analog fluids in rigid curved and straight artery models. *Biorheology* **1990**, *27*, 711–733. [[CrossRef](#)]
14. Vlastos, G.; Lerche, D.; Koch, B. The superposition of steady on oscillatory shear and its effect on the viscoelasticity of human blood and a blood-like model fluid. *Biorheology* **1997**, *34*, 19–36. [[CrossRef](#)]
15. Miller, P. Matching index of refraction using a diethyl phthalate/ethanol solution for in vitro cardiovascular models. *Exp. Fluids* **2006**, *41*, 375–381. [[CrossRef](#)]
16. Torner, B.; Konnigk, L.; Wurm, F.H. Influence of turbulent shear stresses on the numerical blood damage prediction in a ventricular assist device. *Int. J. Artif. Organs* **2019**, *42*, 735–747. [[CrossRef](#)]
17. Thamsen, B.; Blümel, B.; Schaller, J.; Paschereit, C.O.; Affeld, K.; Goubergrits, L.; Kertzsch, U. Numerical Analysis of Blood Damage Potential of the HeartMate II and HeartWare HVAD Rotary Blood Pumps. *Artif. Organs* **2015**, *39*, 651–659. [[CrossRef](#)]
18. Torner, B.; Konnigk, L.; Abroug, N.; Wurm, F.-H. Turbulence and turbulent flow structures in a ventricular assist device-A numerical study using the large-eddy simulation. *Int. J. Numer. Meth. Biomed. Eng.* **2021**, *37*, e3431. [[CrossRef](#)]
19. Oglat, A.A.; Matjafri, M.Z.; Suardi, N.; Abdelrahman, M.A.; Oqlat, M.A.; Oqlat, A.A. A New Scatter Particle and Mixture Fluid for Preparing Blood Mimicking Fluid for Wall Less Flow Phantom. *J. Med. Ultrasound* **2018**, *26*, 134. [[CrossRef](#)]
20. Gonzales-Tello, P.; Camacho, F.; Biazquez, G. Density and Viscosity of Concentrated Aqueous Solutions of Polyethylene Glycol. *J. Chem. Eng. Data* **1994**, *39*, 611–614. [[CrossRef](#)]
21. Bhanot, C. Dynamic viscosity versus probe-reported microviscosity of aqueous mixtures of poly(ethylene glycol). *J. Chem. Thermodyn.* **2012**, *45*, 137–144. [[CrossRef](#)]
22. Cardoso, A.V.; Camargos, A.O. Geometrical Aspects During Formation of Compact Aggregates of Red Blood Cells. *Mater. Res.* **2002**, *5*, 263–268. [[CrossRef](#)]
23. Raymond, A.; Smith, E.R.; Liesegang, J. The physical properties of blood—Forensic considerations. *Sci. Justice J. Forensic Sci. Soc.* **1996**, *36*, 153–160. [[CrossRef](#)] [[PubMed](#)]
24. Ding, J.; Niu, S.; Chen, Z.; Zhang, T.; Griffith, B.P.; Wu, Z.J. Shear-Induced Hemolysis: Species Differences. *Artif. Organs* **2015**, *39*, 795–802. [[CrossRef](#)] [[PubMed](#)]
25. *ASTM F1841-97*; Standard Practice for Assessment of Hemolysis in Continuous Flow Blood Pumps. ASTM International: West Conshohocken, PA, USA, 2017.
26. Gräf, F.; Finocchiaro, T.; Laumen, M.; Mager, I.; Steinseifer, U. Mock circulation loop to investigate hemolysis in a pulsatile total artificial heart. *Artif. Organs* **2015**, *39*, 416–422. [[CrossRef](#)] [[PubMed](#)]
27. Vandenberghe, S.; Segers, P.; Meyns, B.; Verdonck, P. Hydrodynamic Characterisation of Ventricular Assist Devices. *Int. J. Artif. Organs* **2001**, *24*, 470–477. [[CrossRef](#)]
28. Maruyama, T.; Murashige, T.; Sakota, D.; Maruyama, O.; Hijikata, W. Development of an Intelligent Ventricular Assist Device with a Function of Sensorless Thrombus Detection. In Proceedings of the 40th Annual International Conference of the IEEE Engineering in Medicine and Biology Society (EMBC), Honolulu, HI, USA, 18–21 July 2018; pp. 4516–4519.
29. König, C.S.; Clark, C.; Mokhtarzadeh-Dehghan, M.R. Comparison of flow in numerical and physical models of a ventricular assist device using low- and high-viscosity fluids. *Proc. Inst. Mech. Eng.* **1999**, *213*, 423–432. [[CrossRef](#)]
30. *DIN 9906*; Rotodynamic Pumps—Hydraulic Performance Acceptance Test—Grades 1 and 2. 2002, Normenausschuss Maschinenbau (NAM) im DIN Deutsches Institut für Normung e.V. Beuth Verlag GmbH: Berlin, Germany, 2002.
31. ANSYS, Inc. *ANSYS CFX-Modeling Guide 18.0: Chap, 15.3.2*; ANSYS: Canonsburg, PA, USA, 2017.
32. Merrill, E.W. Rheology of blood. *Physiol. Rev.* **1969**, *49*, 863–888. [[CrossRef](#)]
33. Wiegmann, L.; Boës, S.; de Zélicourt, D.; Thamsen, B.; Schmid Daners, M.; Meboldt, M.; Kurtcuoglu, V. Blood Pump Design Variations and Their Influence on Hydraulic Performance and Indicators of Hemocompatibility. *Ann. Biomed. Eng.* **2018**, *46*, 417–428. [[CrossRef](#)]

34. *Operating Instructions HAAKE Mars Rheometer, Version 1.9*; Thermo Scientific: Waltham, MA, USA, 2010.
35. Bundesamt für Gesundheit BAG. 2015. Available online: https://www.bag.admin.ch/dam/bag/de/dokumente/chem/themen-a-z/factsheet-ethylenglykol.pdf.download.pdf/2015-07-20_factsheet_ethylenglykol_de.pdf (accessed on 16 March 2023).

Disclaimer/Publisher's Note: The statements, opinions and data contained in all publications are solely those of the individual author(s) and contributor(s) and not of MDPI and/or the editor(s). MDPI and/or the editor(s) disclaim responsibility for any injury to people or property resulting from any ideas, methods, instructions or products referred to in the content.